2010 IEEE International Conference on Robotics and Automation
Anchorage Convention District
May 3-8, 2010, Anchorage, Alaska, USA

Toward Autonomous Scientific Exploration of Ice-covered Lakes—Field Experiments with the ENDURANCE AUV in an Antarctic Dry Valley

Shilpa Gulati[1, 2, *], Kristof Richmond[1], Christopher Flesher[1], Bartholomew P. Hogan[1], Aniket Murarka[2], Gregory Kuhlmann[2], Mohan Sridharan[3], William C. Stone[1], and Peter T. Doran[4]

[1]Stone Aerospace, Del Valle, TX, USA
[2]The University of Texas at Austin, Austin, TX, USA
[3]Texas Tech University, Lubbock, TX, USA
[4]University of Illinois at Chicago, Chicago, IL, USA

***Abstract*— Chemical properties of lake water can provide valuable insight into its ecology. Lakes that are permanently frozen over with ice are generally inaccessible to comprehensive exploration by humans. This paper describes the integration of several novel and existing technologies into an autonomous underwater robot, ENDURANCE, that was successfully used for gathering scientific data in West Lake Bonney in Taylor Valley, Antarctica, in December 2008.**

This paper focuses on three novel technological and algorithmic solutions. First, a robust position estimation system that uses an acoustic beacon to complement traditional dead-reckoning is described. Second, a novel vision-based docking algorithm for locating and ascending a vertical shaft by tracking a blinking light source is presented. Third, a novel profiling system for measuring water properties while causing minimal water disturbance is described. Finally, experimental results from the scientific missions in 2008 in West Lake Bonney are presented.

I. Introduction

ENDURANCE (Environmentally Non-Disturbing Under-ice Robotic Antarctic Explorer) is a hovering autonomous underwater vehicle. It was developed to perform scientific exploration of ice-covered lakes that are otherwise inaccessible to extensive exploration by humans. ENDURANCE successfully performed a four-week long scientific mission in the west lobe of Lake Bonney in Taylor Valley, one of the McMurdo Dry Valleys in December 2008 [1].

The McMurdo Dry Valleys are the largest ice-free region in Antarctica with a total area of about 4800 km^2. These dry valleys are a polar desert environment with mean annual temperatures of the valley floor between $-30°$C to $-14.8°$C and precipitation of less than 10 cm per year [2]. There are about 20 lakes in the McMurdo Dry Valleys almost all of which maintain a perennial ice-cover (2.8-6.0 m) over liquid water. These lakes are remnants of glacial lakes believed to be as old as 4.6 million years [3].

Lake Bonney consists of two lobes - the west lobe and the east lobe, connected by a channel (Fig. 1(a)). The dimensions of the west lobe are approximately 3 km $\times$ 1.5 km, with a maximum depth of about 40 m. Under the ice cover lies a freshwater lens which extends down to a sharp halocline (a sharp salinity gradient) at a depth of about 12 m [4]. Below the halocline is a salty body of water which reaches a salinity of about four times seawater at its greatest depths. Taylor Glacier, an outlet glacier of the east Antarctic ice sheet, flows into the west end of the west lobe [5].

(a) (b)

Fig. 1. (a) Aerial view of Lake Bonney. ENDURANCE performed scientific exploration of the west in 2008. (b) ENDURANCE being deployed through the melt hole from the mission-control center. The melt hole diameter is only slightly larger than the vehicle diameter leaving a clearance of $\approx$ 30 cm on each side when the vehicle is centered in the hole.

Scientific exploration of West Lake Bonney with ENDURANCE had three primary objectives. First, the chemical properties such as pH, density, electrical conductivity, bioluminescence, etc. had to be measured for the entire west lobe. These properties form a useful basis for understanding the unique ecology and geochemistry of lakes in the Dry Valleys [4], [6]. Second, a high resolution bathymetric map of the underwater part of Taylor glacier face had to be constructed. In addition, visual imaging of the grounding line (the line where glacier meets water) was desired. Third, bathymetric mapping of the lake bottom was required to establish the physical geometry hidden by the ice cover.

In this paper, we describe some of the unique challenges faced in accomplishing the scientific missions and discuss novel technological and algorithmic solutions that were developed to meet these challenges. The solutions presented are applicable to AUV navigation in other ice-covered or otherwise poorly accessible underwater environments.

II. Background and Contributions

Lake Bonney presents a unique and challenging environment for autonomous exploration by a robotic vehicle. The ice-cover on Lake Bonney means that the vehicle must be

*Corresponding author (gulati@mail.utexas.edu).

deployed through a *melt hole* in the lake ice (Fig. 1(b)). The logistics of melting a hole large enough for the vehicle and establishing a mission-control center necessitate that the vehicle start and terminate its missions at a single, fixed location on the lake. This, combined with the extent of the lake, requires that the vehicle perform navigation over a distance of several kilometers and return to within a few meters of the melt hole. Further, after returning to within a few meters of the melt hole, the vehicle is required to locate it and ascend to recharge its batteries and download data. To protect the unique Lake Bonney environment and to obtain reliable water chemistry data, disturbance in the lower saltwater layers must be kept at a minimum during operations. Hence, the vehicle is restricted to operating in the upper freshwater layer.

A variety of robotic vehicles have been deployed for under-ice operations. The Theseus AUV [7] demonstrated early autonomous under-ice cable-laying. The ALTEX [8] successfully gathered mid-water data under Arctic sea ice. The Autosub AUV [9] has performed a number of missions under sea, fast, and shelf ice. The SeaBED [10] and Puma and Jaguar [11] AUVs have explored geothermal vents in the Arctic ocean.

The key differences between these vehicles and ENDURANCE are the very restricted operating volume (between 3 and 12 m depth), the difficult acoustic environment (smooth ice above and halocline below), the requirement to perform precision operations under the ice and near the glacier face, and the extremely limited water access (a single 2 m diameter hole) which demands very robust navigation and an auto-docking capability.

ENDURANCE is a descendant of the DepthX vehicle [12], [13]. A simultaneous localization and mapping (SLAM) algorithm using sonar sensors was successfully tested on DepthX in the confines of flooded shafts [14]. However, the lack of physical features and the significant acoustic multi-path due to the ice roof and the water density profile make sonar SLAM unsuitable in Lake Bonney. Hence, we rely on dead-reckoning for position estimation using a conventional down-looking DVL (Doppler Velocity Log) and an IMU (Inertial Measurement Unit) [13]. In order to provide a fail-safe mechanism for locating and returning to the melt hole, we added an ultra-short baseline (USBL) acoustic positioning system to the navigation sensor suite [15]. This system increases robustness to failure and helps guarantee successful return to the melt hole by providing a complimentary measurement of vehicle position.

The dead-reckoning and USBL system can bring the vehicle to within a few meters of the melt hole. However, completing egress requires a docking algorithm that allows the vehicle to search for and ascend a melt hole with tight clearances. We developed a novel vision-based docking algorithm that uses a blinking light source for docking [16].

The requirement that the lower layers of water be minimally disturbed led us to develop a spooling profiling system that allows the vehicle to remain in the fresh-water layer while an instrument package or *sonde* is spooled all the way down to the lake bottom [17]. This is in contrast to most underwater vehicles that have a body-fixed instrument package (e.g. in [11]). Our profiling system allows the sonde to be accurately positioned in the water column while causing very little disturbance. Further, this system can perform automated sonde drops down to a height of 1 m above the lake bottom.

For the development phase of the ENDURANCE deployment, including 2008 operations at Lake Bonney, an additional measure of safety was provided by a fiber-optic tether connection allowing us to "look over the shoulder" of the robot and manually intervene if necessary, as well as a magnetic beacon system allowing the vehicle to be localized from the surface to within 0.2 m and permitting us to obtain geo-referenced positions of some points with GPS [15].

To summarize, the primary contribution of this work is a successfully deployed robotic system that integrates several novel and existing technologies for exploring and collecting scientific data from an ice-covered lake. First, we present a robust position estimation system that fuses data from DVL, IMU and USBL sensors to guarantee return to the melt hole. Second, we describe a novel vision-based docking algorithm that allows an AUV to find and egress through a melt hole in the ice cover. Third, we present a profiling system that can sample a water column with centimeter-level accuracy while causing minimal disturbance. Field results from experiments conducted over four weeks in West Lake Bonney show that all three systems performed as expected and the vehicle was successful in fulfilling its scientific objectives.

A. Mission Description

The scientific objectives of the 2008 missions were to collect chemical data (profiling), and conduct bathymetric and visual imaging of the lake bottom and glacier face. We describe the profiling missions in some detail here. The details of other missions can be found in [1].

A typical profiling mission consists of the following steps: (i) the vehicle deploys through a melt hole in the lake ice; (ii) it travels to a grid point, turns off its thrusters, and rests quiescently on the underside of the ice; (iii) the profiling system samples the lake water almost down to the lake bottom; (iv) the vehicle moves to the next grid point; (v) after profiling at all grid points, the vehicle returns to its nominal home position beneath the melt hole using dead-reckoning; (vi) the vehicle ascends the melt hole using vision-based docking.

For reliable profiling, the vehicle pose needs to be held stationary. While station-keeping performance was refined to high accuracy and precision in previous experiments [15], an ice-picking technique was chosen instead in Lake Bonney. In this technique, the vehicle is ballasted slightly positively buoyant. When it reaches a grid point, it stops and stabilizes its lateral position, turns off control and floats up until it touches the roof. The underside of ice at Lake Bonney is smooth and provides a stable resting surface. This technique provides the most stable platform for deploying the sonde,

and has the additional advantages of reducing energy usage and increasing the vertical extent of water column sampling.

III. Position Estimation

The position estimation system inherited from DepthX consists of an Inertial Measurement Unit (IMU), a Doppler Velocity Log (DVL) and depth sensors which together provide data for estimating the 6-DOF pose and velocity of the vehicle. The orientation and acceleration measurements from the IMU are fused with bottom-relative velocities from the DVL. The bottom-relative DVL velocity is rotated into world coordinates using the IMU orientation measurements and combined with IMU accelerations in a linear Kalman filter. This has the advantage of allowing the vehicle to operate for several seconds without DVL lock, relying solely on accelerometer readings. The fused, world-frame velocity is then integrated to arrive at the horizontal components of vehicle position. The vertical component is taken from measurements by two 6 mm resolution pressure-depth sensors. The details of dead-reckoning pose-estimation can be found in [18].

This dead-reckoning system is able to provide accuracies of less than 0.2% of distance traveled. However, it faced several challenges in Lake Bonney in guaranteeing safe return of the vehicle to the melt hole. First, an inherent limitation of dead-reckoning is that error in estimated state accumulates as the vehicle moves. For the longest missions (up to 2.5 km), this has the potential to make reaching the melt hole difficult on return, particularly because very little battery energy would be left to execute an extensive search (see Section IV). Second, DVL performance in the acoustically challenging environment was unknown. Position accuracy could be severely affected by degraded DVL measurements or drop-outs due to the difficult acoustic environment or minimum range violations when operating in closed confines.

To make the navigation robust for return to the melt hole, we added an inverted Ultra-Short Baseline (USBL) system to the sensor suite. The USBL is an acoustic positioning system consisting of a transceiver on the AUV which periodically pings a stationary transponder. The transponder immediately responds with its own ping, and based on the measured bearing angle and time-of-flight at the transceiver, the system returns the position of the transponder relative to the vehicle. The USBL operates at a relatively low update rate (every 2-5 s). USBL positioning error is proportional to distance to the transponder (Fig. 2(b)). It provides an absolute reference to the melt hole location, improving as the vehicle nears the transponder location, ensuring safe and swift recovery.

USBL transponder position measurements are first converted to give the vehicle position in world coordinates. These measurements are then filtered for outliers based on a threshold distance from the current best estimate of vehicle position, given the expected range-proportional measurement error. The remaining measurements are then fused with dead-reckoned position in a linear Kalman filter taking into account the accumulated drift error and the USBL measurement error.

A. Results from Field Experiments

Due to a number of logistical delays, USBL position estimates were not fully integrated into the ENDURANCE control system in time for the 2008 Lake Bonney missions. The USBL was used primarily as a backup position sensor in case of failure of other systems. However, USBL data was recorded throughout the missions and an analysis of USBL performance in the Lake Bonney environment was completed.

DVL dead-reckoning was able to provide sufficient accuracy for most missions. However, dead-reckoning failures occurred during Mission 2 (due to bubble formation on the DVL transducers), Mission 15 (due to DVL minimum range violations), and Mission 16 (due to a software failure). When failures did occur, extensive manual intervention was required to safely recover the vehicle, proving the need for the fail-safe security provided by the USBL for fully autonomous operations.

The USBL horizontal position measurement was generally reliable even at the greatest distances from the melt hole ($\approx$650 m). USBL performance degraded in shallow water at the lake edges and near the glacier face and accompanying submerged moraine. In these areas, significant offsets were observed, depending on vehicle orientation (Fig. 2(a)), most likely due to multipath effects from the nearby surfaces. By comparing USBL position measurements to the GPS-corrected dead-reckoning pose measurements, the error distribution in the USBL data can be studied. During operations in Lake Bonney, the USBL achieved a horizontal error distribution, 50% circular error probable (CEP), of approximately 2.5% of range (Fig. 2(b)).

Vertical errors in the USBL position measurements were of much greater magnitude (Fig. 2(c)), displaying a cone-like distribution over several hundred meters as a result of reflections from the overhead ice at 3 m depth and the underlying strong halocline at about 12 m depth (these boundaries essentially act as an acoustic waveguide). As this component of USBL position is ignored, these errors do not affect navigation on ENDURANCE.

Based on the data gathered at Lake Bonney, the performance of the USBL-aided position estimation was evaluated in a post-processing simulation (Fig. 2(d)). For missions performed away from the glacier face, and where USBL position fixes were available during the return, positioning accuracy at the melt hole was improved and was not a function of distance traveled. However, for missions near the glacier face, where operations did not ensure USBL fixes during the return run, accuracy was often degraded, indicating a need for more intelligent filtering of USBL measurements. With full integration into the on-board navigation system, including system calibration and operational modifications, it is anticipated that USBL-aided navigation will improve beyond the results demonstrated in post-processing.

IV. Vision-based Docking

Once the vehicle has reached its nominal home position using the positioning system described in the previous sec-

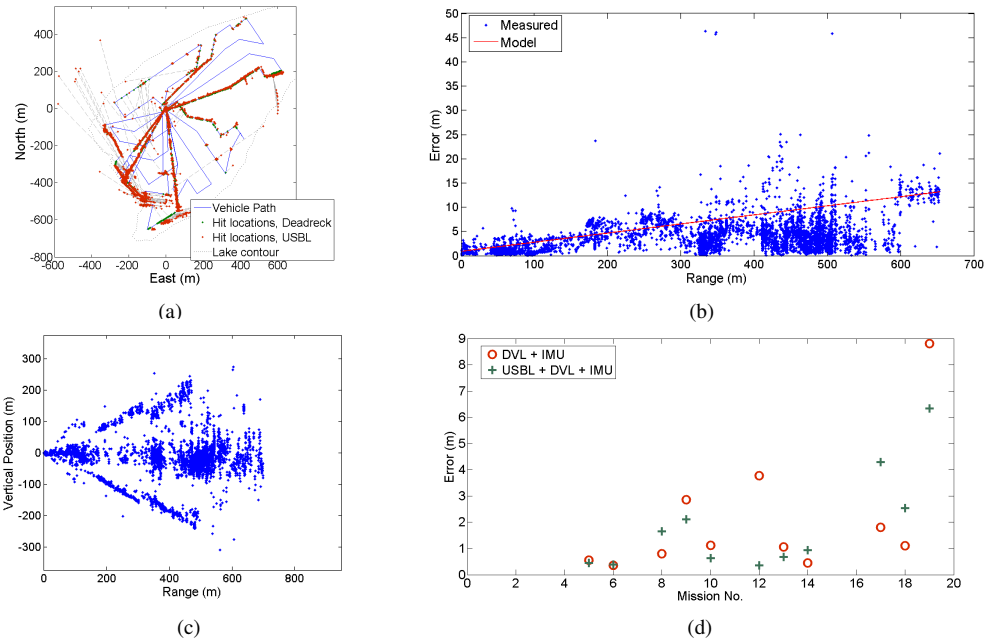

Fig. 2. USBL position estimation performance at Lake Bonney. (a) USBL position measurements plotted along with the IMU + DVL dead-reckoning data. USBL position measurements at the lake margins often displayed large errors as these represent extreme acoustic environments (ice-to-bottom separation of less than 7 m, close proximity to glacier ice face and moraines). (b) USBL horizontal error as a function of range (excluding outliers). The empirical 1-σ error is 0.9 m + 0.019 $\times$ range. (c) Vertical component of USBL position measurement as a function of range. The USBL transponder was deployed at a depth of 8 m, and the vehicle with the transceiver operated between 3.5 m and 8 m. The significantly greater vertical distribution of USBL position measurements is due to the horizontal reflecting layers in Lake Bonney. (d) Comparison of the return-to-hole accuracy of pure dead-reckoning and USBL-aided position, from post-processed data. During early missions (1-14), the vehicle stayed far from the lake margins and the USBL transceiver was pointed toward the transponder during the return. These missions show overall improvement in the position accuracy. During later missions (15-19), the vehicle operated near the glacier face and the transceiver was pointed away from the transponder during the return. These missions show a degradation due to incorporation of systematically erroneous position fixes. Dead-reckoning failed during Missions 2, 15, and 16. Missions 1, 3, 4, and 11 did not record data or were aborted for other reasons.

tion, it ascends the melt hole using vision-based docking. For this, a downward-facing blinking light is suspended roughly centered above the melt hole. A light detection algorithm tracks the light in the images captured by an upward-facing camera mounted on top of the vehicle.

Vision-based docking begins when the vehicle reaches its nominal home position. First, a search behavior is initiated where the vehicle moves in a spiral pattern to look for the light. Next, when the light is detected, an ascent behavior is initiated. Here the vehicle ascends up the melt hole while keeping the light centered in the upward camera images. The coordinates of the light source center are expressed as angles $(\theta_x^t,\ \theta_y^t)$ in the image frame (Fig. 3). The vehicle's control enables it to move independently in the lateral (x, y) plane and the vertical direction (z).

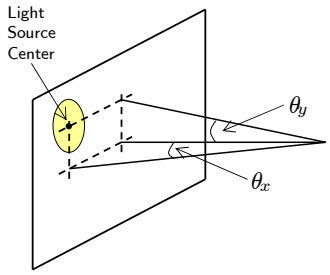

Fig. 3. Coordinates of the light source center are expressed as angles in the image from the upward-facing camera. The light source is not necessarily centered in the image.

- *Spiraling Behavior*: Using dead-reckoned position, the vehicle follows a spiral $r = \frac{b}{2\pi}\theta$ to search for a light source. The parameter b is the distance between the arms of the spiral and is determined from the depth at which the spiral search is performed and the field of view of the camera – b is chosen to ensure that the under-surface of the ice is completely and efficiently scanned by the camera for the light source. The parameter θ is varied from zero to θ_{max} such that a maximum radius of r_{max} is reached. The search radius itself is calculated from the lateral distance traveled by the vehicle and its dead-reckoning accuracy.
- *Ascent/Descent Behavior*: The ascent controller uses a PD control law for lateral velocity control and a PID control law for vertical velocity control. For lateral control $(\theta_x^t,\ \theta_y^t)$ (Fig. 3) is used as the error signal. The control law tries to center the light source in the image thereby centering the robot on the light source. For vertical control, a non-zero z-velocity is commanded only when the light is approximately centered in the image. The ascent controller stops when the vehicle reaches the water surface. For descent, the vehicle uses the same controller as for ascent except that control in the z-direction is disabled. A descent weight is placed on top of the vehicle so that it sinks down the melt hole while being controlled in the x and y directions. When the transit depth is reached, the weight is manually retrieved.

A. Light Detection Algorithm

The controllers described in the previous section require accurate detection and tracking of the target light source in the camera image. At the camera frame rate of around

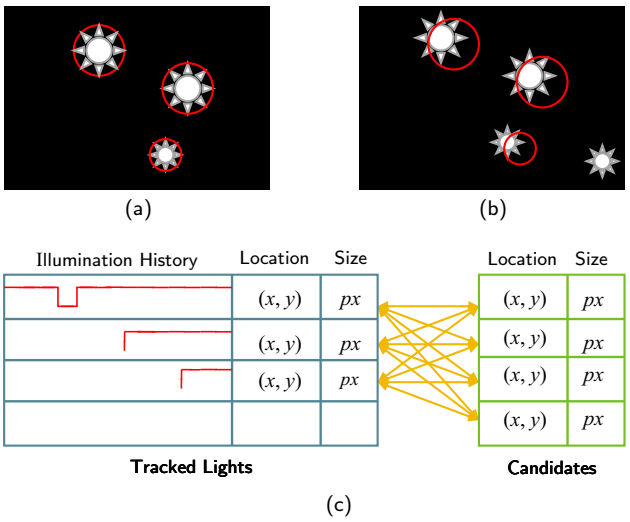

Fig. 4. The set of tracked light sources L is updated when a set of candidate light sources C are identified in a newly captured image frame. This is done by establishing correspondence between tracked light sources and the newly identified candidates. (a) Three light sources are currently being tracked. (b) Four candidates have been identified in the most recent image frame. (c) The process of establishing correspondence begins by constructing a graph that connects each element of L to each element of C where edge weight is the distance between the corresponding tracked and candidate light.

6 Hz, frames are captured and then processed by our low-level vision routines (built on the OpenCV image processing library [19]) to identify high-contrast contours as candidates for the target light. These contours are then filtered based on their roundness and size to eliminate obvious false positives. For each candidate contour that passes the filters, we pass the center and radius of the bounding circle to the light tracking algorithm.

The light detection algorithm must perform robustly in the presence of ambient light sources, such as direct light from the sun and indirect reflections from the ice. To distinguish the target light source from these persistent sources, we track the target's unique blinking signature. Our novel solution does not require synchronization between the camera and light, and only makes the straightforward assumption that the vehicle does not move too quickly from frame to frame.

Our tracking algorithm extends the point-correspondence method of Salari and Sethi [20] to track blinking lights in addition to persistent lights in the presence of occlusion. The algorithm maintains a set, L, which contains the current light sources being tracked, including their bounding circles and *histories*. A history is a list that contains whether or not the light source was seen or unseen for each frame going back to some upper bound on the history length (24 frames in our experiments). The algorithm updates this data structure by incorporating C, the set of candidate light sources seen in the current frame (Fig. 4). The tracker must identify which candidates correspond to light sources that have already been seen and which candidates are new. We take a greedy edge-elimination approach as illustrated in Fig. 5.

The algorithm begins by computing a matrix containing the distances between all currently tracked light sources and the candidates in the frame (Fig. 5(a)). The first round of elimination removes all edges with distance greater than a

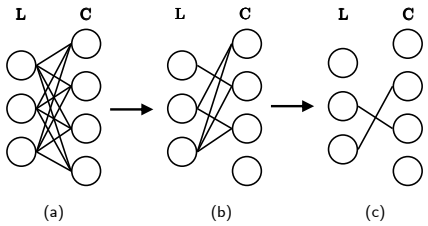

Fig. 5. (a) To process new candidate light sources, the light-detection algorithm begins with a complete bipartite graph between the set of candidates (C) and the set of currently tracked light sources (L). (b) Next, edges are removed if the distance between the sources is too large or if the disparity in their sizes is too high. (c) Finally, edges are removed in order from greatest distance to smallest, while not removing edges ($l \in L, c \in C$) if doing so would orphan both l and c at the same time.

threshold of 10° in the camera's field of view. This threshold was determined experimentally, and depends on the vehicle's speed and expected minimum distance to the target. We set this threshold large enough to allow the robot to move some significant amount between frames, but small enough to avoid clumping all light sources together. At the same time, we eliminate edges if they connect light sources with drastically different sizes. The primary motivation for this filter is to prevent specular glare on the light source glass from being recognized as the light when it is off, a problem we encountered during early experimentation.

After the first culling, the edges that remain appear as depicted in Fig. 5(b). Notice that some nodes still have more than one edge, which means that there are multiple potential matches to be made. The next round of elimination determines which of those potential matches is best. The algorithm sorts the remaining edges by decreasing distance and then eliminates them one-by-one. An edge will not be eliminated if it is the only edge remaining for the nodes it connects, because that edge is treated as a correct match.

Finally, the graph that results from the greedy culling algorithm is shown in Fig. 5(c). No node has more than one edge. The edges that remain connect the candidates in the current frame with their corresponding light source histories. Orphaned nodes in L (one in the figure) are tracked light sources that were not seen in the current frame. Their histories are updated to reflect that they were unseen. Orphaned nodes in C (two in the figure) are newly-observed candidates, which are added to the list of tracked light sources with a fresh history.

With L updated, we compute a score for each tracked light source. After some experimentation with alternatives, the score that worked best was the number of transitions. Every time the light switches from seen to unseen or unseen to seen in its bounded history, that light source receives a point. The highest possible score, then, is half the history length. In practice, however, a true positive tends to score in the 3–7 range. Through informal experimentation, we arrived at a value of 4 for the minimum threshold value on the score. Thus, the light source with the highest score above threshold is returned as the target. If no light sources score above the threshold, then the algorithm returns a null value.

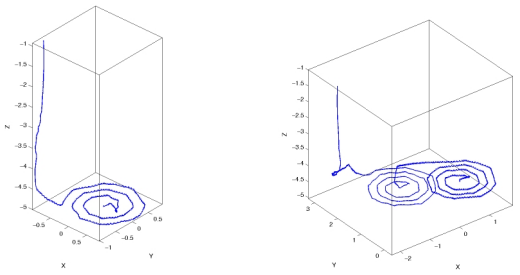

(a) ascent-10 (b) ascent-9

Fig. 6. Plots showing the vehicle's path for two ascents once the visual homing algorithm starts. (a) The robot searches spirally for the light source; once it locks onto the light source, the robot begins to rise while staying centered on the light. (b) The robot fails to find the light the first time it spirals. It then drifts for a short distance before the visual homing algorithm is restarted, the robot finds the light source, and rises.

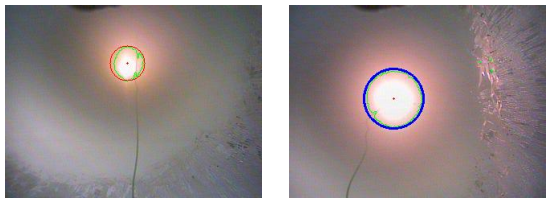

(a) (b)

Fig. 7. Sequence of images taken by the upward-facing camera during Mission 3 showing various stages of the visual homing behavior. (a) During search, the light-detection module identifies a candidate light source (red circle). Note that the light source is not centered in the image. (b) After observing the light source blink a few times, the source is confirmed as the desired target (blue circle). The robot also starts centering the light source in the image.

B. Results from Field Experiments

Visual homing was used for 10 missions in West Lake Bonney with the ascent behavior being used all 10 times and descent used 8 times. Spiraling behavior was executed in 5 ascents. Twice the vehicle was farther from the melt hole than could be reached with a single spiral search. Here, spiral search was executed multiple times by manually issuing a command through the user-interface. The transit depth of the vehicle was 5 m and hence most ascents were initiated at a depth of 5 m.

For all the 18 instances, visual homing was successful in guiding the vehicle up or down the melt hole without collisions with the walls. Fig. 6 shows the path of the vehicle for two ascents. Fig. 7 shows some images taken by the upward-facing camera during an ascent. The spiral search proved to be a simple yet effective way to search for the light source.

1) Ascent/Descent Controller Precision: We analyze the precision of the ascent controller by measuring the overall standard deviation in the vehicle's x and y coordinates after it has approximately centered itself with respect to the light source and starts rising. We analyze data for 7 missions for which both image and pose data is available.

To compute the overall standard deviation we first normalize all x and y values for each mission by their means. If $\overline{x}$ is the mean x coordinate for an ascent/mission, then the normalized value $\widehat{x}$ for a particular x coordinate is given by $\widehat{x} = x - \overline{x}$. The normalized values are combined into a single vector and the overall precision is then given by the vector's standard deviation. The overall precision for the y coordinates is similarly computed.

The overall value for the standard deviation is 5.70 cm in the x direction and 4.60 cm in the y direction. The vehicle has a clearance of 10 cm on all sides when it is in the melt hole implying that for about 92% of the time, the vehicle was fairly well centered in the melt hole and not touching any walls. Qualitatively, the vehicle came up the melt hole successfully every time without suffering any damage, suggesting that at worst the vehicle only lightly grazed the melt hole walls. Thus, the controller and the light detection algorithm were able to successfully surface the robot. The precision for the descents is numerically similar to that for the ascents.

2) Light Detection Accuracy: To evaluate algorithm performance, we are primarily interested in four criteria. First, the algorithm should acquire and detect the blinking light quickly. Second, it should not lose track of the light once it has been acquired, producing false negatives. Third, it should not produce false positives by misclassifying non-target light sources. And fourth, it should maintain an accurate estimate of the target center.

For seven separate ascents of the vehicle, we evaluated the light tracking algorithm against these criteria. Our performance metrics require a comparison with the true location of the target light source. Without access to ground truth, we approximated the location of the target light source by hand-labeling the images in our data set. For each frame in which the true target light source was present, we manually recorded the pixel location that appeared to be closest to the center of the target. We then ran the same images through the light-detection algorithm and computed the error in this estimate along with several other statistics. The complete results are shown in Table I.

The first statistic, "Total frames", is the number of frames stored by the camera from the time the first candidate light source is identified until the vehicle completes ascent. Although the camera operated at 30 Hz, images were stored at about 6 Hz, recording roughly every fifth frame. Thus, for example, for an ascent that lasts around 30 s, roughly 180 frames would be recorded.

The next metric, "Acquisition time", is the number of frames between the first candidate light and the first identified blinking target. If the target is lost after initial acquisition, then we consider that a "Drop". We record the number of drop occurrences and the total duration (in frames) over the occurrences. We do the same for "Misclassifications", which are instances when the algorithm locks on to the incorrect light source. Finally, we measure the Euclidean distance (in pixels) between the true target position and the algorithm output. Because misclassifications have a large impact on this metric, we record two versions of this statistic: one with misclassified instances included, and one without.

From Table I it is clear that the algorithm performed well during the Lake Bonney deployment. In only one of the seven ascents did the algorithm ever encounter any drops

Ascent No.	3	5	8	9	10	12	13
Total frames	190	278	243	150	193	179	153
Acquisition time (frames)	21	12	162	101	123	95	8
Number of Drops	1	0	0	0	0	0	0
Total drop time (frames)	11	0	0	0	0	0	0
Number of Misclassifications	1	0	0	0	0	0	0
Misclassification time (frames)	15	0	0	0	0	0	0
Average distance (pixels)	11.2	1.91	3.63	4.44	2.24	3.02	3.38
Avg. dist. w/o misclassified (pixels)	2.83	1.91	3.63	4.44	2.24	3.02	3.38

TABLE I

STATISTICS EVALUATING BLINKING LIGHT TRACKER ALGORITHM ACROSS SEVEN SEPARATE ASCENTS AT LAKE BONNEY.

or misclassifications. Also, the low-level contour algorithm appears to have done a good job of finding the centers of the light sources, as is evidenced by the average distance values.

V. PROFILING SYSTEM

Once the vehicle reaches a grid point, water properties are sampled with a profiling system. The profiling system consists of three main components—the spooler, the sonde and the electronic-control housing (Fig. 8). The spooler is a servo-driven winch. We designed the servo controllers to achieve precise control over payload position and speed. The sonde has nine instruments which measure conductivity, temperature, pressure, pH, oxidation-reduction potential (ORP), chlorophyll, turbidity, chromatic dissolved organic matter (CDOM), and ambient light. In addition, the sonde has a high-definition camera, a high power LED light, a bottom ranging altimeter, and an on-board lithium battery. A electro-mechanical Kevlar reinforced cable connects the sonde to the electronics-control housing. The electronics-control housing contains communications, power, servo-control and logic components.

Automated profiling begins when the vehicle ice-picks at a grid point. Once the vehicle's position has stabilized, a pre-programmed sequence is initiated where the sonde is smoothly spooled down to a height of 1 m above the lake bottom. Altimeter readings are used for position estimation in this process. The LED lights are switched on and the high-definition camera takes a sequence of pictures (see Fig. 9) of the lake bottom while the sonde is slowly moved up 1 m. The sonde is then smoothly spooled back up and stowed in the vehicle.

A. Results from Field Experiments

The profiling system was tested in various facilities, including the Neutral Buoyancy Lab (NBL) at Johnson Space center. One of the issues faced at NBL was that the altimeter on the sonde gave erroneous readings while close to the pool surface. Once a few meters down, the readings were accurate and enabled automated sonde drops down to a height of 1 m above the pool floor. However, in Lake Bonney, because of soft lake floor and multipath due to halocline and ice roof, we encountered altimeter dropouts of variable duration during sonde drops. This precluded us from using the profiler in the automated mode. Instead, we relied on spooling down the sonde by manually issuing commands to the servos. In the future, we plan to fix this problem by integrating information from multiple sensors such as the down looking DVL, the servo encoders, and the altimeter for robust position estimation.

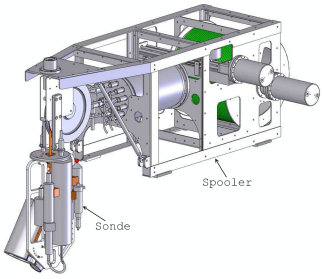

Fig. 8. The profiling system hardware. The sonde consists of various instruments that measure water properties. A high-definition camera is also part of the sonde. The sonde is smoothly lowered or raised with a winch-based spooler.

ENDURANCE performed profiling at 108 points in West Lake Bonney during 2008 missions. The data from each sonde drop included chemical property data (Fig. 10(a)) sampled at a resolution of 0.1 m in depth, and lake-bottom images (Fig. 10(b)).

VI. CONCLUSIONS

ENDURANCE was the first entity (human or robot) to extensively explore the sub-ice world of West Lake Bonney and gather a large amount of scientific data. A total of 19 sub-ice missions were performed by ENDURANCE in 2008, including 8 profiling missions with 108 sonde drops (Fig. 11) and 5 glacier mapping missions. At Lake Bonney, the dead-reckoning system with IMU and downward-facing DVL demonstrated a 50% CEP drift error of about 0.1% of distance traveled. USBL positioning demonstrated 50% CEP errors of 2.5% of range, and demonstrated the ability to improve position accuracy and serve as a fail-safe system to improve system autonomy. The vision-based docking algorithm was successfully used a total of 18 times for ascent and descent. Quantitative and qualitative results show that the light-detection is robust and the ascent/descent controller is sufficiently precise to keep the vehicle centered more than 90% of the time. The profiler performed smoothly with no serious issues in the harsh environment. ENDURANCE returned to West Lake Bonney in the austral summer of 2009 to continue its scientific missions.

VII. ACKNOWLEDGMENTS

ENDURANCE was a NASA sponsored research activity, funded through the ASTEP program office, NASA Science

(a) (b)

Fig. 9. A profiling operation, captured by under-water cameras at the Neutral Buoyancy Lab (NBL) at Johnson Space Center. Initially, the sonde is stowed in the vehicle. (a) During profiling, the sonde is smoothly spooled down. (b) When the sonde reaches a height of 1 m above the floor, a camera takes images of the floor.

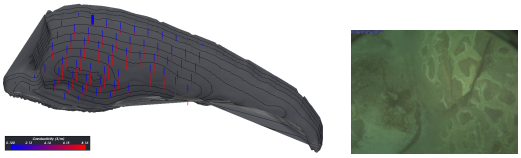

(a) (b)

Fig. 10. Examples of data collected during the profiling missions. (a) Plot of conductivity data measured by the sonde. Plot thanks to the Electronic Visualization Lab at the University of Illinois at Chicago [21]. (b) Microbial mats are visible in an image taken by the sonde camera. Such mats were usually seen on the lake bottom in shallow coastal regions.

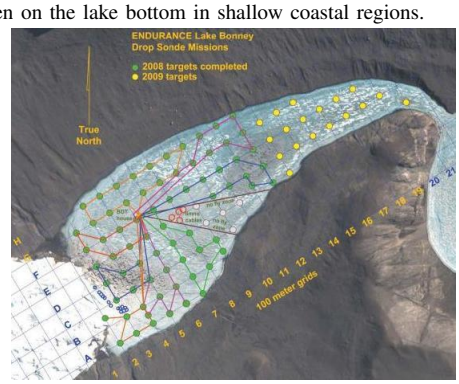

Fig. 11. Summary of profiling missions. Green circles mark the locations of successful sonde drops during the 2008 season. Different colored lines show different missions. The longest mission length was ≈1800 m.

Directorate under grant NNX07AM88G. Peter Doran at the University of Illinois at Chicago is the principal investigator. The authors would like to thank John Priscu at Montana State University; Andrew Johnson, Maciej Obryk, Shriram Iyer, and Alessandro Febretti at the University of Illinois at Chicago.

Logistical support in Antarctica was provided by the National Science Foundation through the U.S. Antarctic Program. The authors would also like to thank the Center for Limnology at the University of Wisconsin at Madison, the Hyde Park Baptist Church at The Quarries in Austin, Texas, and the Sonny Carter Training Facility Neutral Buoyancy Lab at NASA Johnson Space Center, for their enthusiastic support of the ENDURANCE test program.

REFERENCES

[1] W. C. Stone, B. Hogan, C. Flesher, S. Gulati, K. Richmond, A. Murarka, G. Kuhlman, M. Sridharan, V. Siegel, R. M. Price, P. Doran, and J. Priscu, "Sub-ice exploration of West Lake Bonney: ENDURANCE 2008 mission," in *International Symposium on Unmanned Untethered Submersible Technology (UUST)*, 2009.

[2] P. T. Doran, C. P. McKay, G. D. Clow, G. L. Dana, A. G. Fountain, T. Nylen, and W. B. Lyons, "Valley floor climate observations from the McMurdo dry valleys, Antarctica," *Journal of Geophysical Research*, vol. 107, 2002.

[3] P. T. Doran, R. A. W. J. 1, and W. B. Lyons, "Paleolimnology of the McMurdo Dry Valleys, Antarctica," *Journal of Paleolimnology*, vol. 10, pp. 85–114, 1994.

[4] J. C. Priscu, "The biogeochemistry of nitrous oxide in permanently ice-covered lakes of the McMurdo Dry Valleys, Antarctica," *Global Change Biology*, vol. 3, pp. 301–315, 1997.

[5] A. G. Fountain, W. B. Lyons, M. B. Burkins, G. L. Dana, P. T. Doran, K. J. Lewis, D. M. McKnight, D. L. Moorhead, A. N. Parsons, J. C. Priscu, D. H. Wall, R. A. W. Jr., , and R. A. Virginia, "Physical controls on the Taylor Valley Ecosystem, Antarctica," *BioScience*, vol. 49, no. 12, pp. 961–971, 1999.

[6] W. B. Lyons and S. K. F. K. A.Welch, "History of McMurdo Dry Valley lakes, Antarctica, from stable chlorine isotope data," *Geology*, vol. 27, no. 6, pp. 527–530, 1999.

[7] J. M. Thorleifson, L. T. C. Davies, M. R. Black, D. A. Hopkin, and R. I. Verrall, "The Theseus autonomous underwater vehicle: A Canadian success story," in *Proceedings of the OCEANS 97 Conference*, vol. 2. Halifax, Nova Scotia: MTS/IEEE, Oct. 6–9 1997, pp. 1001–1006.

[8] R. McEwen, H. Thomas, D. Weber, and F. Psota, "Performance of an AUV navigation system at arctic latitudes," in *Proceedings of the OCEANS 2003 Conference*. San Diego, CA: MTS/IEEE, Sept. 22–27 2003.

[9] S. McPhail, "Autosub operations in the Arctic and Antarctic," in *Proceedings of the Masterclass in AUV Technology for Polar Science*, G. Griffiths and K. Collins, Eds., National Oceanography Centre, Southampton, UK. Society for Underwater Technology, Mar. 28–30 2006, pp. 27–38.

[10] M. V. Jakuba, C. N. Roman, H. Singh, C. Murphy, C. Kunz, C. Willis, T. Sato, and R. A. Sohn, "Long-baseline acoustic navigation for under-ice autonomous underwater vehicle operations," *Journal of Field Robotics*, no. 25, pp. 861–879, 2008.

[11] C. Kunz, C. Murphy, H. Singh, C. Pontbriand, R. A. Sohn, S. Singh, T. Sato, C. Roman, K. Nakamura, M. Jakuba, R. Eustice, R. Camilli, and J. Bailey, "Toward extraplanetary under-ice exploration: Steps in the Arctic," *Journal of Field Robotics*, vol. 26, no. 4, pp. 411–429, Apr. 2009.

[12] N. Fairfield, D. Jonak, G. A. Kantor, and D. Wettergreen, "Field results of the control, navigation and mapping system of a hovering AUV," in *International Symposium on Unmanned Untethered Submersible Technology (UUST)*, 2007.

[13] N. Fairfield, G. Kantor, D. Jonak, and D. Wettergreen, "DEPTHX autonomy software: Design and field results," Carnegie Mellon University, Tech. Rep. CMU-RI-TR-08-09, 2008.

[14] N. Fairfield, G. A. Kantor, and D. Wettergreen, "Real-time SLAM with octree evidence grids for exploration in underwater tunnels," *Journal of Field Robotics*, vol. 24, pp. 3–21, 2007.

[15] K. Richmond, S. Gulati, C. Flesher, B. P. Hogan, and W. C. Stone, "Navigation, control, and recovery of the ENDURANCE under-ice hovering AUV," in *International Symposium on Unmanned Untethered Submersible Technology (UUST)*, 2009.

[16] A. Murarka, G. Kuhlmann, S. Gulati, M. Sridharan, C. Flesher, and W. C. Stone, "Vision-based frozen surface egress: A docking algorithm for the ENDURANCE AUV," in *International Symposium on Unmanned Untethered Submersible Technology (UUST)*, 2009.

[17] B. P. Hogan, C. Flesher, and W. C. Stone, "Development of a sub-ice automated profiling system for Antarctic lake deployment," in *International Symposium on Unmanned Untethered Submersible Technology (UUST)*, 2009.

[18] G. A. Kantor, N. Fairfield, D. Jonak, and D. Wettergreen, "Experiments in navigation and mapping with a hovering AUV," in *International Conference on Field and Service Robotics*, 2007.

[19] "OpenCV," http://opencv.willowgarage.com/.

[20] V. Salari and I. K. Sethi, "Feature point correspondence in the presence of occlusion," *IEEE Transactions on Pattern Analysis and Machine Learning*, vol. 12, no. 1, pp. 87–91, 1990.

[21] A. Johnson, "Homepage of Andrew Johnson at University of Illionois at Chicago," http://www.evl.uic.edu/aej, 2009.